Optimal conditions for the Bell test using spontaneous parametric down-conversion sources

Yoshiaki Tsujimoto,[1] Kentaro Wakui,[1] Mikio Fujiwara,[1] Kazuhiro Hayasaka,[1] Shigehito Miki,[2,3] Hirotaka Terai,[2] Masahide Sasaki,[1] and Masahiro Takeoka[1]

[1]*Advanced ICT Research Institute, National Institute of Information and Communications Technology (NICT), Koganei, Tokyo 184-8795, Japan*

[2]*Advanced ICT Research Institute, National Institute of Information and Communications Technology (NICT), 588-2 Iwaoka, Iwaoka-cho, Nishi-ku, Kobe 651-2492, Japan*

[3]*Graduate School of Engineering, Faculty of Engineering, Kobe University, 1-1 Rokko-dai cho, Nada-ku, Kobe 657-0013, Japan*

(Received 16 October 2018; published 26 December 2018)

We theoretically and experimentally investigate the optimal conditions for the Bell experiment using spontaneous parametric down-conversion (SPDC) sources. In theory, we show that a relatively large average photon number (typically $\sim$0.5) is desirable to observe the maximum violation of the Clauser-Horne-Shimony-Holt (CHSH) inequality. Moreover, we show that the violation converges to 0.27 in the limit of large average photon number. In experiment, we perform the Bell experiment without postselection using polarization-entangled photon pairs at 1550-nm telecommunication wavelength generated from SPDC sources. While the violation of the CHSH inequality is not directly observed due to the overall detection efficiencies of our system, the experimental values agree well with those obtained by the theory with experimental imperfections. Furthermore, in the range of small average photon numbers ($\leqslant$0.1), we propose and demonstrate a method to estimate the ideal CHSH value intrinsically contained in the tested state from the lossy experimental data without assuming the input quantum state.

DOI: 10.1103/PhysRevA.98.063842

I. INTRODUCTION

Quantum-mechanically entangled photon pairs are essential tools for various optical quantum information and communication protocols [1,2]. Such entangled photon pairs can be generated with spontaneous parametric down-conversion (SPDC). To generate perfectly correlated pairs via the SPDC process, which is probabilistic, it is frequently driven by a weak pumping regime such that the emitted light contains only biphotons (a pair of single photons) and higher-order multiphoton emissions are sufficiently low. This feature is useful when one makes postselection of the coincidence photon counting events.

The weakly pumped SPDC source has also been used in the experiment *without* postselection. One important example is a loophole-free test of the Bell inequality [3,4]. Violation of the Bell inequality rules out the possibility of describing the correlation between two parties by the local hidden variable model. To observe the genuine quantum correlation directly, it is important that the Bell test is performed without any loopholes, e.g., the detection loophole. In addition, the loophole-free Bell test implies new quantum information applications, such as device-independent quantum key distribution (DIQKD) [5,6] and random number generation [7]. So far, in photonic systems, the violation of the Bell inequality closing the detection and locality loopholes [8–11] has been demonstrated by combining the weakly pumped SPDC sources and highly efficient detectors.

Though these experiments successfully violate the Clauser-Horne-Shimony-Holt (CHSH) inequality [12], the amount of violation was limited to be small ($\sim 10^{-4}$) compared to the maximal violation of $2\sqrt{2}-2 \sim 0.83$, since the weakly pumped SPDC source mainly emits vacuum and only a few biphotons. The average photon number is typically in the order of 10^{-2}. That is, the major component of the quantum state is vacuum, which does not contribute to yield the violation of the CHSH inequality. In contrast, when the SPDC source is pumped strongly, higher-order multiphoton emissions also suppress the violation, which indicates that there is an optimal balance between a vacuum component and multiphoton components. In fact, very recently, larger violations of the CHSH inequality have been reported by using SPDC sources with a relatively strong pump which produce a non-negligible amount of multiple pairs [13,14]. Moreover, the theoretical analysis [15] considering multiphoton pair emissions of the SPDC sources indicates that the achievable violations of the CHSH inequality are 0.30 in single-mode case and 0.35 in multimode case, which means that the experimental violations are still far from the theoretical limits. (Note that the model in Ref. [15] can reproduce the experimental violations when taking the experimental parameters into account.)

In this paper, we further investigate this direction in detail both theoretically and experimentally to clarify the optimal parameters of the SPDC sources that maximize the violation of the CHSH inequality. First we perform theoretical simulations based on the characteristic function approach, which can take account of higher-order multiphoton pair emissions [16,17]. Then we show the optimal parameters for the system for a given detection efficiency (η) in detail, especially the optimal average photon numbers (λ) of the two SPDC sources and their relative ratio. It is revealed that the

maximal violation is obtained at the relatively high average photon number regime, where the contribution of multiphoton pair emissions is not negligible: $\lambda > 0.1$ in most cases, and $\lambda = 0.99$ is optimal for $\eta = 1$. Surprisingly, the violation of the CHSH inequality does not vanish, even for larger λ in the single-mode case, whereas the SPDC source emits mostly multiphoton pairs in this regime. We show that the violation converges to 0.27 in the limit of large λ, which is almost comparable to the maximal violation with the same source (=0.31). We also show that the measurement angle of the Bell test is almost independent of the detection efficiency. It is noteworthy that this feature allows us to reduce the number of optimization parameters and therefore is practically useful for saving computational resources.

Second, to test the theoretical predictions, we perform the Bell-test experiment without postselections using polarization-entangled photon pairs generated by SPDC. We collected all the events, including no-detection (vacuum) events, and calculated the CHSH value for each average photon number. While the overall detection efficiencies of our system are insufficient to directly observe the violation of the CHSH inequality, the CHSH values obtained by the experiment agree well with the theory in a wide range of parameters. Furthermore, for the low average photon number regime of $\lambda \leqslant 0.1$, we propose and demonstrate a method to estimate the ideal probability distributions of the Bell test from the lossy experimental data without assuming the input quantum state. The results agree with the theory and thus provide a useful estimation technique for quantum optics experiments with a certain amount of losses.

The paper is organized as follows. In Sec. II, we briefly review the Bell test using SPDC sources and describe our theoretical model, including higher-order photon numbers and experimental imperfections. In Sec. III, we present our numerical results. The experimental setup is described in Sec. IV. In Sec. V, we present our experimental results and introduce the method to compensate the loss of the system. We conclude the paper in Sec. VI.

II. BELL TEST VIA THE SPDC SOURCES

The schematic diagram of the Bell test is shown in Fig. 1(a). A pair of particles is distributed from the source to two receivers, Alice and Bob. They randomly choose the measurement settings, $X_i \in \{X_1, X_2\}$ and $Y_j \in \{Y_1, Y_2\}$, respectively. All the observables produce binary outcomes $a_i, b_j \in \{-1, +1\}$. Alice and Bob repeat the measurement and calculate the CHSH value

$$S = \langle a_1 b_1 \rangle + \langle a_2 b_1 \rangle + \langle a_1 b_2 \rangle - \langle a_2 b_2 \rangle, \tag{1}$$

where $\langle a_i b_j \rangle = P(a = b|X_i, Y_j) - P(a \neq b|X_i, Y_j)$. Here, $S > 2$ indicates that the particles shared between Alice and Bob possess nonlocal quantum correlation which cannot be reproduced by any local hidden variables. The maximal value of S allowed by quantum mechanics is $2\sqrt{2}$, which is known as the Cirelson bound [18] and achieved by using a maximally entangled pair.

Next, the realistic model of the Bell test with SPDCs is shown in Fig. 1(b). The SPDCs emit entangled photon pairs, or more precisely, the two-mode squeezed vacuum (TMSV)

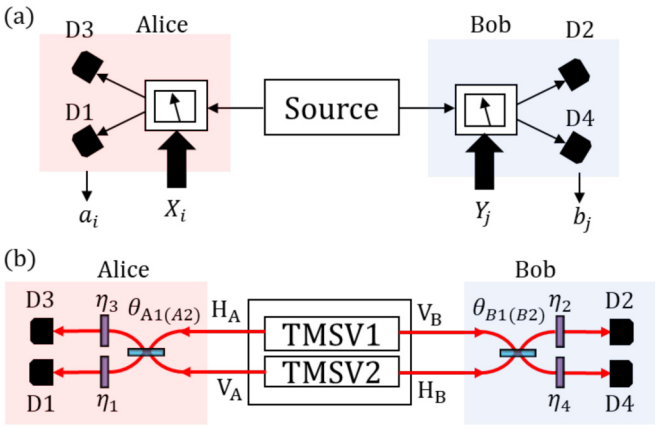

FIG. 1. (a) The schematic diagram for the Bell experiment. Alice and Bob share a pair of particles and choose the measurement settings $X_i \in \{X_1, X_2\}$ and $Y_j \in \{Y_1, Y_2\}$, respectively. The measurement outcomes are binary, i.e., $a_i, b_j \in \{-1, +1\}$. (b) The realistic model for the Bell experiment. An entangled photon pair is generated by means of a pair of two-mode squeezed vacua (TMSV) over polarization modes. The polarization measurement is realized by the polarization mixing followed by the on-off type, single-photon detectors with dark counts.

whose Hamiltonian is represented by $\hat{H} = i\hbar(\zeta_1 \hat{a}^\dagger_{H_A} \hat{a}^\dagger_{V_B} + \zeta_2 \hat{a}^\dagger_{V_A} \hat{a}^\dagger_{H_B} - \text{H.c.})$, where $\hat{a}^\dagger_j$ is the photon creation operator in mode j and $\zeta_k = |\zeta_k| e^{i\phi_k}$ is the coupling constant of TMSVk ($k = 1, 2$), which is proportional to the complex amplitude of each pump. In the following, ϕ_k is fixed as $\phi_1 = 0$ and $\phi_2 = \pi$. H and V denote the horizontal and vertical polarizations, respectively. The generated quantum state is described by

$$|\Psi_{\text{ent}}\rangle = \exp(-i\hat{H}t/\hbar)|0\rangle \tag{2}$$

$$= \sum_{n=0}^{\infty} \frac{1}{\cosh r_1 \cosh r_2} \sqrt{n+1} |\Phi_n\rangle, \tag{3}$$

where

$$|\Phi_n\rangle = \frac{(-i)^n}{n!\sqrt{n+1}} (\tanh r_1 \hat{a}^\dagger_{H_A} \hat{a}^\dagger_{V_B} - \tanh r_2 \hat{a}^\dagger_{V_A} \hat{a}^\dagger_{H_B})^n |0\rangle. \tag{4}$$

Here $|0\rangle$ is the vacuum state, and $r_k = |\zeta_k| t$ is the squeezing parameter of TMSVk. Note that the average photon number of TMSVk is given by $\lambda_k = \sinh^2 r_k$. The state clearly consists of an infinite series, and the contribution from higher-order photon numbers cannot be negligible, even with finite λ_k. The polarizer with angle θ works as a polarization-domain beam-splitter mixing the H and V modes, where its transmittance and reflectance are $\cos^2\theta$ and $\sin^2\theta$, respectively. The overall detection efficiencies, including the system transmittance and the imperfect quantum efficiencies of the detectors, are denoted by η_l for $l = 1, 2, 3, 4$. This is modeled by inserting the losses in each arm before the detectors with unit efficiency [see Fig. 1(b)]. We consider that the detectors D1, D2, D3, and D4 are on-off–type, single-photon detectors which only distinguish between vacuum (off: no-click) and nonvacuum (on: click). Dark count, which is a wrong click of the detector, is also taken into account in the model.

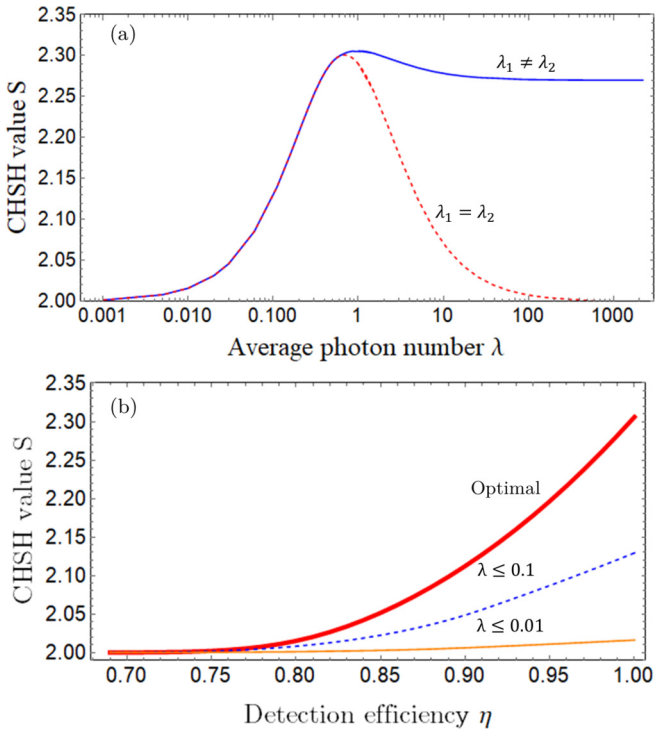

FIG. 2. (a) Log-linear plot of the average photon number λ vs S. For each point we fix λ and optimize the other parameters. (b) The overall detection efficiency η vs S for the three different ranges of λ. For each η we fix the ranges of λ and perform optimizations.

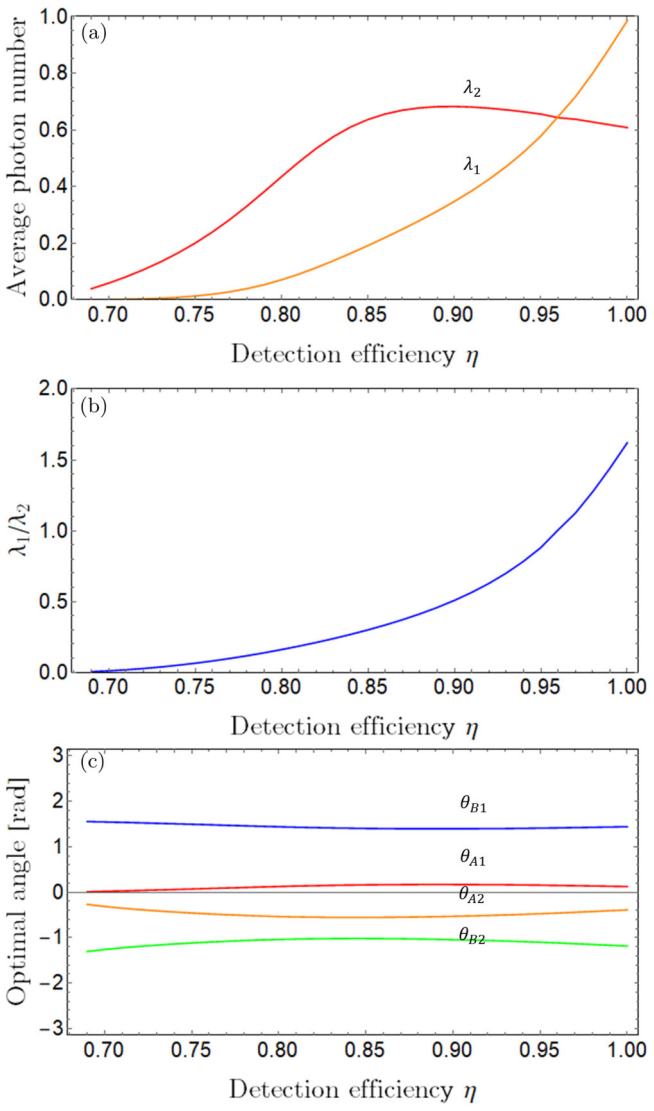

FIG. 3. (a) The overall detection efficiency η vs the optimal average photon numbers (λ_1 and λ_2). (b) η vs λ_1/λ_2. (c) η vs the optimal angles of the polarizers. In the simulations, we assume that $\eta := \eta_1 = \eta_2 = \eta_3 = \eta_4$ and $\nu = 0$.

III. NUMERICAL RESULTS

To numerically calculate S in Eq. (1) with the above SPDC model, we use the approach based on the characteristic function [16,17]. This approach is applicable when the system is composed of Gaussian states and operations, and on-off detectors. The Gaussian state is defined by the state whose characteristic function (or equivalently, Wigner function) has a Gaussian distribution, including TMSV states. The Gaussian operation is also defined as an operation transforming a Gaussian state to another Gaussian state, which includes the operations by linear optics and second-order nonlinear processes. The setup in Fig. 1(b) includes only these means and thus meets the condition above. See Appendix and Ref. [16] for more details of this approach. Note that a similar calculation with a different approach is reported in Ref. [15].

We calculate the probability of all the combinations of the photon detection (click) and no-detection (no-click) events for each polarizer angle and obtain the probability distributions. We denote, for example, the probability of observing clicks in D1 and D2, and no-clicks in D3 and D4 as $P(\mathrm{c1}, \mathrm{c2}, \mathrm{nc3}, \mathrm{nc4})$. Each Alice and Bob determines her or his local rule and assigns $+1$ or -1 for each detection event. Since there are four possible local events for each Alice and Bob, i.e., (i) only the one detector clicks, (ii) only the other detector clicks, (iii) both of the two detectors simultaneously click, and (iv) no detector clicks, there are 16 possible choices for each Alice and Bob to assign ± 1. We introduce the following simple local assignment strategy for Alice (Bob): only D1(D2) clicks $\rightarrow -1$ and otherwise $\rightarrow +1$, respectively. We note that this local rule is only related to the optimal measurement angles and does not affect the maximum violation and the optimal input quantum state. Under the condition that Alice (Bob) chooses the angle $\theta_{A1}(\theta_{B1})$, respectively, the probability that both Alice and Bob obtain the outcome -1 is calculated by $P(-1,-1|\theta_{A1},\theta_{B1}) = P(\mathrm{c1}, \mathrm{c2}, \mathrm{nc3}, \mathrm{nc4})$. Similarly, the other conditional probabilities $P(+1,-1|\theta_{A1},\theta_{B1})$, $P(-1,+1|\theta_{A1},\theta_{B1})$, and $P(+1,+1|\theta_{A1},\theta_{B1})$ are also calculated by the detection probabilities, which enables us to calculate S. See Appendix for the details of the formulas.

Figure 2(a) shows the relation between the average photon number and S in an ideal system, where all the detection efficiencies are unity and detectors have no dark counts (i.e., $\eta_1 = \eta_2 = \eta_3 = \eta_4 = 1$ and $\nu = 0$). We define $\lambda := \max\{\lambda_1, \lambda_2\}$, and then for given λ, numerically optimize the other average photon number and $\{\theta_{A1(B1)}, \theta_{A2(B2)}\}$ via the Nelder-Mead

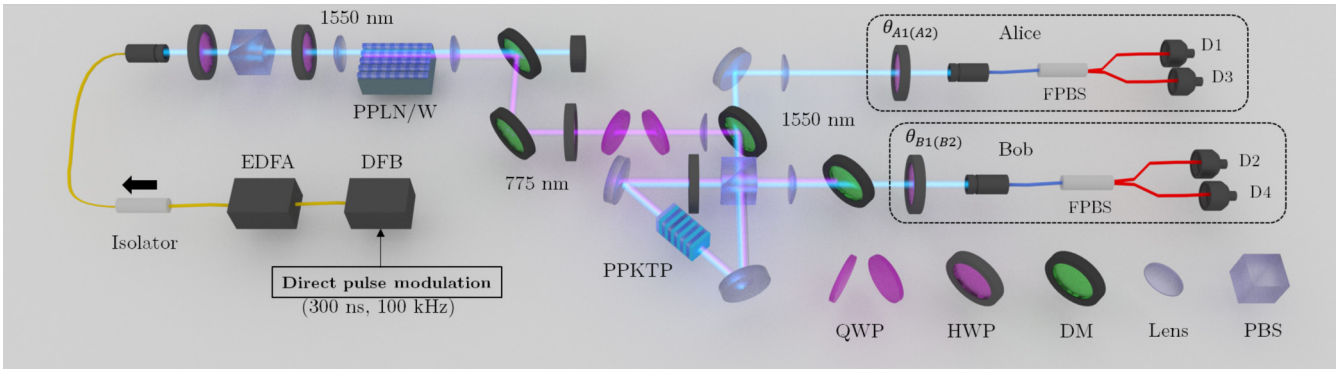

FIG. 4. The setup for the Bell experiment. To generate entangled photon pairs by SPDC, we used counterpropagating pump pulses to excite the PPKTP crystal in the Sagnac loop interferometer. Alice and Bob choose the measurement angles $\{\theta_{A1}, \theta_{A2}\}$ and $\{\theta_{B1}, \theta_{B2}\}$, respectively, and assign $+1$ or -1 for each detection event to calculate the S value. DFB: distributed feedback laser, EDFA: erbium-doped fiber amplifier, PPLN/W: periodically poled lithium niobate waveguide, PPKTP: periodically poled potassium titanyl phosphate, QWP: quarter-waveplate, HWP: half-waveplate, DM: dichroic mirror, PBS: polarization beamsplitter, FPBS: fiber-based PBS.

method such that S is maximized. The blue solid curve shows the optimal values of S. The maximum value is around 2.31, which coincides with the theoretical result by Vivoli *et al.* [15]. We find that the maximum violation is obtained at $\lambda = 0.99$, which is much larger than those used in the previous experiments [8–11]. Rather surprisingly, the blue solid curve converges to 2.27 as λ becomes larger, while the smaller average photon number is almost constant at around 0.70. This is contrasted with the multimode case [13,14] where the violation vanishes in the limit of large λ. The red dashed curve shows the optimized S under the restriction of $\lambda := \lambda_1 = \lambda_2$. It takes a maximum value of 2.30 at around $\lambda = 0.66$ and then monotonically decreases as λ becomes larger.

Next, we show the loss tolerance of S for the three different ranges of λ in Fig. 2(b). In the simulation, we assumed that $\eta := \eta_1 = \eta_2 = \eta_3 = \eta_4$ and $\nu = 0$. λ_1, λ_2 and the measurement angles are optimized for each η. The red thick curve, blue dashed curve, and yellow thin curve represent S optimized under the conditions of $0 \leqslant \lambda$, $0 \leqslant \lambda \leqslant 0.1$, and $0 \leqslant \lambda \leqslant 0.01$, respectively. The figure shows that the limited λ strongly restricts the maximum S in any η. The result indicates that the maximum S obtainable in the previous Bell experiments using SPDC sources with small λ is intrinsically limited and thus suggests a use of higher pumping of the SPDC sources to obtain a larger CHSH violation.

Finally, we show the optimal parameters for a given η in Figs. 3(a)–3(c). The optimal average photon numbers are shown in Fig. 3(a). Even when $\eta = 1$, the two optimal average photon numbers are unbalanced. The ratio between λ_1 and λ_2 is shown in Fig. 3(b). We found that the ratio of λ_1/λ_2 monotonically and continuously decreases as η decreases. This result qualitatively agrees with the analysis based on qubit systems in Ref. [19]. The optimal angles of the polarizers are shown in Fig. 3(c). Interestingly, the optimal angles are almost constant regardless of η.

IV. EXPERIMENTAL SETUP

Theoretical predictions in the above section are verified using the experimental setup illustrated in Fig. 4. We choose the measurement angles as $\{\theta_{A1}, \theta_{A2}\} = \{0, \pi/5\}$ and $\{\theta_{B1}, \theta_{B2}\} = \{3\pi/5, -3\pi/5\}$, by which S is expected to be $S = 2.30$ with $\lambda_1 = \lambda_2 = 0.62$ when the overall detection efficiency is unity and the dark count probabilities are zero. These angles are slightly different from those shown in Fig. 3(b) since we apply the condition $\lambda_1 = \lambda_2$ for simplicity. A distributed feedback (DFB) laser generates pulsed light at 1550 nm. The DFB laser is directly modulated by electrical pulses with 100-kHz repetition and 300-ns duration. The output laser pulse is amplified by an erbium-doped fiber amplifier (EDFA). The output of EDFA is vertically polarized by a half-waveplate (HWP) and a polarizing beamsplitter (PBS), and then coupled to the 34-mm-long, type-0, periodically poled lithium niobate waveguide (PPLN/W) for second harmonic generation (SHG). Amplified spontaneous emission from the EDFA and unconverted fundamental light of the SHG are removed by the dichroic mirrors (DMs). The polarization of the SHG pulses are adjusted by using a HWP and a pair of quarter-waveplates (QWPs). The maximum pulse energy (average power) of our SHG pulses is 0.2 μJ (20 mW). To generate polarization-entangled photon pairs by the SPDC process, SHG pulses are used to pump a 30-mm-long, type-II, periodically poled potassium titanyl phosphate (PPKTP) crystal in a Sagnac loop interferometer with a PBS [20]. The two-qubit component of the generated state forms a maximally entangled state $|\Psi^-\rangle = (|HV\rangle - |VH\rangle)/\sqrt{2}$, where $|H\rangle$ and $|V\rangle$ denote the H and V polarization state of a single photon, respectively. One half of the photon pair passes through the DM and goes to Alice's side while the other photon goes to Bob's side. Alice and Bob set measurement angles $\{\theta_{A1}, \theta_{A2}\}$ and $\{\theta_{B1}, \theta_{B2}\}$, respectively, by means of the HWPs and fiber-based PBSs (FPBSs). Finally, the photons are detected by four superconducting single-photon detectors (SSPDs), D1 and D3 for Alice, and D2 and D4 for Bob, respectively. The quantum efficiencies of these SSPDs are around 75% [21]. The dark count probabilities of the SSPDs are 3.0×10^{-4} per a detection window of 300 ns, corresponding to the pulse duration. The modulation signal for the DFB laser is also used as a starting signal for a time-to-digital converter (TDC), and the detection signals from D1, D2, D3, and D4 are used as stop signals of the TDC. All combinations of click and no-click events are collected without postselection. We assign events

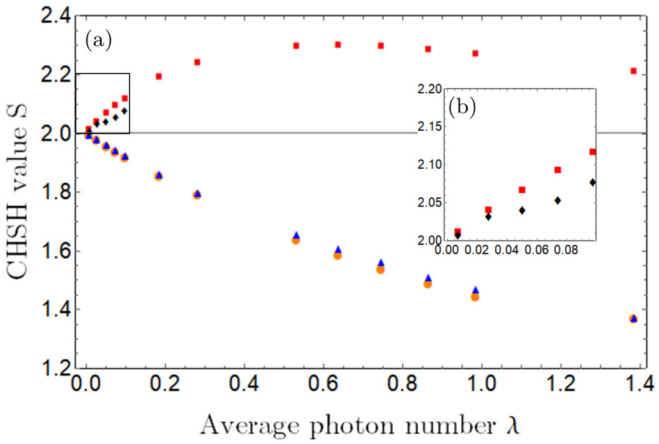

FIG. 5. (a) The S values obtained by the theory with unity detection efficiencies (red square), the theory with experimental parameters (yellow circle), and the experimental results (blue triangle) for the various values of λ. The black diamonds represent the S values obtained by compensating the losses of the system in the range of $\lambda \leqslant 0.1$. (b) The enlarged figure of the enclosed part.

of D1 (D2) clicks on Alice's (Bob's) side as -1 and all the others as $+1$, then calculate S.

V. EXPERIMENTAL RESULTS

Before performing the Bell-test experiment, we estimate the overall detection efficiencies η_l. Suppose a TMSV is detected by two detectors, D1 and D2. The overall detection efficiencies of the two modes (η_1 and η_2) are well estimated by the following equation [22]:

$$\eta_{1(2)} = \frac{C_{12}}{S_{2(1)}}. \tag{5}$$

Here C_{12} is the coincidence count between D1 and D2, and $S_{2(1)}$ is the single-detection count at D2(1). Note that the average photon number of the TMSV photons is small enough for this measurement. In our theoretical model shown in Fig. 1(b), we have assumed the same detection efficiencies for TMSV1 and TMSV2. Thus, in the experiment we carefully align the optical system such that the overall detection efficiencies for TMSV1 and TMSV2 are the same as each other. We estimated them as $\eta_1 = 10.48 \pm 0.69\%$, $\eta_2 = 12.76 \pm 0.97\%$, $\eta_3 = 12.72 \pm 0.53\%$, and $\eta_4 = 11.86 \pm 0.24\%$.

Once η_l is estimated, the average photon number (λ_k) of TMSVk is calculated by using the following relation:

$$\frac{S_{1(2)}}{N} = \frac{\lambda_k \eta_{1(2)}}{1 + \lambda_k \eta_{1(2)}}, \tag{6}$$

where N is the number of the total events, which corresponds to the number of the start signals of the TDC.

In the Bell-test experiment, the difference between λ_1 and λ_2 is set to be less than 1%. Thus we denote $\lambda := \lambda_1 = \lambda_2$ in the following. The results of the Bell experiment are shown in Fig. 5(a). We perform the Bell experiment for various values of λ by changing the energy of the pump pulse. Though the overall detection efficiencies of our system are not in the range of directly observing the CHSH violation, it is still possible to compare our experimental results and the theory calculated with experimentally observed parameters: the average photon numbers, measurement angles, detection efficiencies, and dark counts. The experimental results (blue triangles) and theoretical values with experimental parameters (yellow circles) are in good agreement for each λ, which indicates that the theoretical model well explains the experimental results.

In the low average photon number regime ($\lambda \leqslant 0.1$), it is possible to compensate the imperfection of the overall detection efficiencies *without* assuming the quantum states distributed to Alice and Bob. In other words, one can estimate the intrinsic nonlocality that could be observed with the unity detection efficiencies. Under the assumption that each detector detects at most one photon, the experimentally obtained probability distribution $\boldsymbol{P}_{\rm exp} = (p_1, p_2, \ldots, p_{16})^T$ composed of the 16 combinations of the detection probabilities and the ideal probability distribution with the unity detection efficiencies $\boldsymbol{Q}_{\rm ideal} = (q_1, q_2, \ldots, q_{16})^T$ are connected by the linear transmission matrix $\boldsymbol{T}$ as

$$\boldsymbol{P}_{\rm exp} = \boldsymbol{T}\,\boldsymbol{Q}_{\rm ideal} \tag{7}$$

for each measurement setting. Here, $p_1 = P$(nc1,nc2,nc3,nc4), $p_2 = P$(c1,nc2,nc3,nc4), and so on. $\boldsymbol{T}$ is the upper triangular matrix whose matrix elements are composed of the products of η_l and $(1 - \eta_l)$. For example, the fourfold coincidence probabilities p_{16} and q_{16} are connected by $p_{16} = q_{16} \prod_{l=1}^{4} \eta_l$. One may think that $\boldsymbol{Q}_{\rm ideal}$ is estimated by simply calculating $\boldsymbol{Q}_{\rm ideal} = \boldsymbol{T}^{-1}\boldsymbol{P}_{\rm exp}$. However, in this case, the elements of $\boldsymbol{Q}_{\rm ideal}$ could be negative since $\boldsymbol{P}_{\rm exp}$ contains experimental errors. Thus we determine the most likely elements of $\boldsymbol{Q}_{\rm ideal}$ such that the L^2 distance between $\boldsymbol{P}_{\rm exp}$ and $\boldsymbol{T}\,\boldsymbol{Q}_{\rm ideal}$ is minimum under the condition that $q_i \geqslant 0$ and $\sum_{i=1}^{16} q_i = 1$. Namely, we estimate the probability distribution $\boldsymbol{Q}_{\rm ideal}$ which minimizes the function

$$\sum_{i=1}^{16} \left(p_i - \sum_{j=1}^{16} T_{ij} q_j \right)^2. \tag{8}$$

The S values calculated by $\boldsymbol{Q}_{\rm ideal}$ are shown in Figs. 5(a) and 5(b) by the black triangles. The results agree with but are slightly below the theory plots for the ideal state and detectors (red square), which reflects the deviation of the generated state from ideal TMSVs due to experimental imperfections. In particular, these two plots start to deviate at $\lambda > 0.05$, where the probability of detecting multiphotons at each detector starts to be non-negligible.

VI. CONCLUSION

In conclusion, we theoretically and experimentally investigate the optimal conditions for the Bell test with SPDC sources. We perform the numerical simulation, including multiphoton emissions from the SPDC sources and various imperfections, and see the maximal violation of the CHSH inequality as $S = 2.31$, which agrees with the previous result in Ref. [15]. Then we show the optimal experimental parameters to maximize the CHSH values for a given average photon number of TMSVs or the overall detection efficiency

by numerical simulations. In particular, we show the CHSH value takes its maximum when the average photon number is much larger than those utilized in the previous experiments [8–10]. Interestingly, it is found that the maximum violation of the CHSH inequality converges to 0.27 when one of the two average photon numbers is extremely large. This result indicates that the violation of the CHSH inequality is not determined by a mere trade-off between the amount of vacuum and multiple pairs in the single-mode case. Next, we perform the Bell-test experiment without postselection using polarization-entangled photon pairs generated by SPDC to test these theoretical predictions. The experimentally obtained CHSH values agree well with those obtained by the theory. Moreover, in the range of small average photon numbers, we also propose and demonstrate a method to estimate the CHSH value of the quantum state before undergoing losses by compensating the detection losses without assuming the input quantum state. The result shows good agreement with the theoretical model in the range of $\lambda \leqslant 0.1$. This approach is useful in estimating the properties of quantum states via imperfect detectors.

ACKNOWLEDGMENTS

We thank Kaushik P. Seshadreesan for helpful discussions. This work was supported by JST CREST Grant No. JPMJCR1772, and MEXT/JSPS KAKENHI Grants No. JP18K13487, No. JP17K14130, and No. 17K05091.

APPENDIX: DETAILED CALCULATIONS BASED ON THE CHARACTERISTIC FUNCTION

We describe a procedure to calculate the probability distributions and the CHSH value S using the theoretical model given in Sec. II. First, we review the basic tools used in the characteristic function approach which is often used in Gaussian continuous-variable quantum systems. This method allows us to deal with the quantum state generated by the SPDC process without the need for any approximations such as photon number truncation. Next, we present the method to calculate the detection probabilities. Finally, we describe the procedure to calculate S using the obtained probability distribution.

1. Preliminary

a. Characteristic function

Let us consider N bosonic modes associated with a tensor product Hilbert space $\mathcal{H}^{\otimes N} = \bigotimes_{j=1}^{N} \mathcal{H}_j$, where $\mathcal{H}_j$ is an infinite-dimensional Hilbert space. We define annihilation and creation operators corresponding to each mode as $\hat{a}_j$ and $\hat{a}_j^\dagger$, respectively. They satisfy the commutation relation given by

$$[\hat{a}_j, \hat{a}_k^\dagger] = \delta_{jk}. \tag{A1}$$

We also define the quadrature operators of a bosonic mode as

$$\hat{x}_j = \frac{1}{\sqrt{2}}(\hat{a}_j + \hat{a}_j^\dagger), \tag{A2}$$

$$\hat{p}_j = \frac{1}{\sqrt{2}i}(\hat{a}_j - \hat{a}_j^\dagger). \tag{A3}$$

Note that we choose as a convention $\hbar = \omega = 1$. Their commutation relation is calculated as

$$[\hat{x}_j, \hat{p}_k] = i\delta_{jk}. \tag{A4}$$

We define a density operator acting on $\mathcal{H}^{\otimes N}$ as $\hat{\rho}$. The characteristic function of $\hat{\rho}$ is defined by

$$\chi(\xi) = \mathrm{Tr}[\hat{\rho}\hat{\mathcal{W}}(\xi)], \tag{A5}$$

where

$$\hat{\mathcal{W}}(\xi) = \exp(-i\xi^T \hat{R}) \tag{A6}$$

is the Weyl operator. Here, $\hat{R} = (\hat{x}_1, \ldots, \hat{x}_N, \hat{p}_1, \ldots, \hat{p}_N)^T$ and $\xi = (\xi_1, \ldots, \xi_{2N})^T$ are a $2N$ vector consisting of quadrature operators and a $2N$ real vector, respectively.

b. Gaussian states

A Gaussian state is a quantum state whose characteristic function has a Gaussian distribution:

$$\chi(\xi) = \exp\left(-\frac{1}{4}\xi^T \gamma \xi - i d^T \xi\right), \tag{A7}$$

where γ is a $2N \times 2N$ matrix called the covariance matrix and d is a $2N$-dimensional vector known as the displacement vector. The covariance matrix of the TMSV state generated by a SPDC source is given by

$$\gamma^{\mathrm{TMSV}}(\lambda) = \begin{bmatrix} \gamma^+(\lambda) & \mathbf{0} \\ \mathbf{0} & \gamma^-(\lambda) \end{bmatrix}, \tag{A8}$$

where

$$\gamma^\pm = \begin{bmatrix} 2\lambda + 1 & \pm 2\sqrt{\lambda(\lambda+1)} \\ \pm 2\sqrt{\lambda(\lambda+1)} & 2\lambda + 1 \end{bmatrix}, \tag{A9}$$

while $d = 0$. As is described in Sec. II, $\lambda = \sinh^2 r$ corresponds to the average photon number per mode.

c. Gaussian unitary operations

A Gaussian unitary operation is defined as a unitary operation transforming a Gaussian state to another Gaussian state, which includes the operations by linear optics and the second-order nonlinear process. Any Gaussian unitary operation acting on a Gaussian state is characterized by the following symplectic transformations:

$$\gamma \to S^T \gamma S, \quad d \to S^T d, \tag{A10}$$

where S is a symplectic matrix corresponding to the Gaussian unitary operation. The symplectic matrix for a beamsplitter on mode A and mode B is given by

$$S_{AB}^t = \begin{bmatrix} \sqrt{t} & \sqrt{1-t} & 0 & 0 \\ -\sqrt{1-t} & \sqrt{t} & 0 & 0 \\ 0 & 0 & \sqrt{t} & \sqrt{1-t} \\ 0 & 0 & -\sqrt{1-t} & \sqrt{t} \end{bmatrix}, \tag{A11}$$

where t is the transmittance of the beamsplitter. Hereafter, we simplify the description of a block-diagonalized matrix like

Eq. (A11) as

$$S_{AB}^{t} = \begin{bmatrix} \sqrt{t} & \sqrt{1-t} \\ -\sqrt{1-t} & \sqrt{t} \end{bmatrix}^{\oplus 2}. \tag{A12}$$

d. Measurements

We consider that the detectors D1, D2, D3, and D4 in Fig. 1(b) are on-off type, single-photon detectors, namely, they only distinguish between vacuum and nonvacuum. Denoting the dark count probability of the detectors by ν, the POVM elements of the on-off detectors are described by

$$\hat{\Pi}^{\text{off}}(\nu) = (1-\nu)|0\rangle\langle 0| \tag{A13}$$

and

$$\hat{\Pi}^{\text{on}}(\nu) = \hat{I} - \hat{\Pi}^{\text{off}}(\nu), \tag{A14}$$

where $\hat{I}$ is the identity operator. The detection probability is calculated by introducing the characteristic functions of the positive operator-valued measure (POVM) elements. Similar to the state, the characteristic function of the POVM element $\hat{\Pi}$ is given by $\chi_{\Pi}(\xi) = \text{Tr}[\hat{\Pi}\hat{\mathcal{W}}(\xi)]$. When a single-mode Gaussian state $\hat{\rho}$ with characteristic function $\chi_{\rho}(\xi) = \exp(-\frac{1}{4}\xi^{T}\gamma\xi)$ is measured, the detection probability is given by

$$\begin{aligned} P_{\text{on}} &= \text{Tr}[\hat{\rho}\hat{\Pi}^{\text{on}}] = 1 - (1-\nu)\text{Tr}[\hat{\rho}|0\rangle\langle 0|] \\ &= 1 - \frac{2(1-\nu)}{\sqrt{\det(\gamma + I)}}. \end{aligned} \tag{A15}$$

e. Linear loss

The linear photon losses in the system, such as a coupling efficiency to the single-mode fiber and imperfect quantum efficiency of the detectors, are modeled by performing a beamsplitter transformation of transmittance t between the lossy mode and a vacuum mode, and tracing out the vacuum mode. The transformation of the linear loss on the state with covariance matrix γ can be described as

$$\mathcal{L}^{t}\gamma = K^{T}\gamma K + \alpha, \tag{A16}$$

where $K = \sqrt{t}I$ and $\alpha = (1-t)I$.

2. Detection probabilities

Using the above basic tools, we present the procedure to calculate the detection probabilities. As shown in Fig. 1(b), the entangled photon pair source consists of two TMSV sources over polarization modes. The covariance matrix of the output state is given by

$$\gamma_{H_A V_A H_B V_B}^{\text{TMSV12}} = \begin{bmatrix} 2\lambda_1+1 & 2\sqrt{\lambda_1(\lambda_1+1)} & 0 & 0 \\ 2\sqrt{\lambda_1(\lambda_1+1)} & 2\lambda_1+1 & 0 & 0 \\ 0 & 0 & 2\lambda_2+1 & -2\sqrt{\lambda_2(\lambda_2+1)} \\ 0 & 0 & -2\sqrt{\lambda_2(\lambda_2+1)} & 2\lambda_2+1 \end{bmatrix}^{\oplus 2}. \tag{A17}$$

Note that the relative phase between TMSV1 and TMSV2 is set to π as described in Eq. (4). In the experiment, the two TMSV sources are embedded in the Sagnac loop. In this case, the covariance matrix of the output state is transformed into [16]

$$\gamma_{H_A V_A H_B V_B}^{\text{SL}} = \begin{bmatrix} 2\lambda_1+1 & 0 & 0 & 2\sqrt{\lambda_1(\lambda_1+1)} \\ 0 & 2\lambda_2+1 & -2\sqrt{\lambda_2(\lambda_2+1)} & 0 \\ 0 & -2\sqrt{\lambda_2(\lambda_2+1)} & 2\lambda_2+1 & 0 \\ 2\sqrt{\lambda_1(\lambda_1+1)} & 0 & 0 & 2\lambda_1+1 \end{bmatrix}^{\oplus 2}. \tag{A18}$$

The covariance matrix in Eq. (A18) is first transformed by the (polarization-domain) beamsplitter operations $S_{H_A V_A}^{\theta_A} S_{H_B V_B}^{\theta_B}$. The covariance matrix after the transformation is given by

$$\gamma_{H_A V_A H_B V_B}^{\text{BS}} := S_{H_B V_B}^{\theta_B T} S_{H_A V_A}^{\theta_A T} \gamma_{H_A V_A H_B V_B}^{\text{SL}} S_{H_A V_A}^{\theta_A} S_{H_B V_B}^{\theta_B}. \tag{A19}$$

The overall system losses, including imperfect quantum efficiencies of the detectors, are considered by performing linear-loss operations $\mathcal{L}_{H_A}^{\eta_1}$, $\mathcal{L}_{V_A}^{\eta_3}$, $\mathcal{L}_{H_B}^{\eta_2}$, and $\mathcal{L}_{V_B}^{\eta_4}$ on corresponding modes. The covariance matrix just before the detectors is given by

$$\gamma_{H_A V_A H_B V_B}^{\text{final}} = \mathcal{L}_{H_A}^{\eta_1}\mathcal{L}_{V_A}^{\eta_3}\mathcal{L}_{H_B}^{\eta_2}\mathcal{L}_{V_B}^{\eta_4}\gamma_{H_A V_A H_B V_B}^{\text{BS}} \tag{A20}$$

$$= K_{H_A V_A H_B V_B}^{\eta_1\eta_3\eta_2\eta_4 T}\gamma_{H_A V_A H_B V_B}^{\text{BS}} K_{H_A V_A H_B V_B}^{\eta_1\eta_3\eta_2\eta_4} + \alpha_{H_A V_A H_B V_B}^{\eta_1\eta_3\eta_2\eta_4}, \tag{A21}$$

where

$$K_{H_A V_A H_B V_B}^{\eta_1\eta_3\eta_2\eta_4} = \begin{bmatrix} \sqrt{\eta_1} & 0 & 0 & 0 \\ 0 & \sqrt{\eta_3} & 0 & 0 \\ 0 & 0 & \sqrt{\eta_2} & 0 \\ 0 & 0 & 0 & \sqrt{\eta_4} \end{bmatrix}^{\oplus 2} \tag{A22}$$

and

$$\alpha^{\eta_1\eta_3\eta_2\eta_4}_{H_AV_AH_BV_B} = \begin{bmatrix} 1-\eta_1 & 0 & 0 & 0 \\ 0 & 1-\eta_3 & 0 & 0 \\ 0 & 0 & 1-\eta_2 & 0 \\ 0 & 0 & 0 & 1-\eta_4 \end{bmatrix}^{\oplus 2}. \tag{A23}$$

The detection probabilities are calculated by performing $\hat{\Pi}^{\mathrm{on/off}}(\nu)$ on corresponding modes. For example, the probability of observing clicks in D1 and D2 and no-clicks in D3 and D4 is given by

$$P(\mathrm{c1},\mathrm{c2},\mathrm{nc3},\mathrm{nc4}|\theta_A,\theta_B) = \mathrm{Tr}\left[\rho^{\gamma^{\mathrm{final}}_{H_AV_AH_BV_B}}\hat{\Pi}^{\mathrm{on}}_{H_A}(\nu)\hat{\Pi}^{\mathrm{on}}_{H_B}(\nu)\hat{\Pi}^{\mathrm{off}}_{V_A}(\nu)\hat{\Pi}^{\mathrm{off}}_{V_B}(\nu)\right] \tag{A24}$$

$$= \mathrm{Tr}\left[\rho^{\gamma^{\mathrm{final}}_{H_AV_AH_BV_B}}(\hat{I}-(1-\nu)|0\rangle\langle 0|_{H_A})(\hat{I}-(1-\nu)|0\rangle\langle 0|_{H_B})(1-\nu)|0\rangle\langle 0|_{V_A}(1-\nu)|0\rangle\langle 0|_{V_B}\right] \tag{A25}$$

$$= \frac{4(1-\nu)^2}{\sqrt{\det\left(\gamma^{\mathrm{final}}_{V_AV_B}+I\right)}} - \frac{8(1-\nu)^3}{\sqrt{\det\left(\gamma^{\mathrm{final}}_{H_AV_AV_B}+I\right)}} - \frac{8(1-\nu)^3}{\sqrt{\det\left(\gamma^{\mathrm{final}}_{H_BV_AV_B}+I\right)}} + \frac{16(1-\nu)^4}{\sqrt{\det\left(\gamma^{\mathrm{final}}_{H_AV_AH_BV_B}+I\right)}}, \tag{A26}$$

where $\gamma^{\mathrm{final}}_{V_AV_B}$, $\gamma^{\mathrm{final}}_{H_AV_AV_B}$, and $\gamma^{\mathrm{final}}_{H_BV_AV_B}$ are the submatrices of $\gamma^{\mathrm{final}}_{H_AV_AH_BV_B}$.

3. Calculation of S

As in Eq. (1), S is obtained by calculating $P(a=b|\theta_{A_i},\theta_{B_j})$ and $P(a\neq b|\theta_{A_i},\theta_{B_j})$ for $i,j=\{1,2\}$. For simplicity, omitting the conditions of the angles, these conditional probabilities are given by

$$P(a=b) = P(+1,+1)+P(-1,-1) \tag{A27}$$

and

$$P(a\neq b) = P(+1,-1)+P(-1,+1). \tag{A28}$$

In our model, each probability in the right-hand side of Eqs. (A27) and (A28) is calculated as follows:

$$P(-1,-1) = P(\mathrm{c1},\mathrm{c2},\mathrm{nc3},\mathrm{nc4}), \tag{A29}$$

$$P(+1,-1) = P(\mathrm{c1},\mathrm{c2},\mathrm{c3},\mathrm{nc4})+P(\mathrm{nc1},\mathrm{c2},\mathrm{c3},\mathrm{nc4})+P(\mathrm{nc1},\mathrm{c2},\mathrm{nc3},\mathrm{nc4}), \tag{A30}$$

$$P(-1,+1) = P(\mathrm{c1},\mathrm{c2},\mathrm{nc3},\mathrm{c4})+P(\mathrm{c1},\mathrm{nc2},\mathrm{nc3},\mathrm{c4})+P(\mathrm{c1},\mathrm{nc2},\mathrm{nc3},\mathrm{nc4}), \tag{A31}$$

$$P(+1,+1) = 1-P(-1,-1)-P(+1,-1)-P(-1,+1). \tag{A32}$$

[1] P. Kok, W. J. Munro, K. Nemoto, T. C. Ralph, J. P. Dowling, and G. J. Milburn, Rev. Mod. Phys. **79**, 135 (2007).

[2] J.-W. Pan, Z.-B. Chen, C.-Y. Lu, H. Weinfurter, A. Zeilinger, and M. Żukowski, Rev. Mod. Phys. **84**, 777 (2012).

[3] J. Bell, Physics **1**, 195 (1964).

[4] N. Brunner, D. Cavalcanti, S. Pironio, V. Scarani, and S. Wehner, Rev. Mod. Phys. **86**, 419 (2014).

[5] A. Acín, N. Brunner, N. Gisin, S. Massar, S. Pironio, and V. Scarani, Phys. Rev. Lett. **98**, 230501 (2007).

[6] S. Pironio, A. Acín, N. Brunner, N. Gisin, S. Massar, and V. Scarani, New J. Phys. **11**, 045021 (2009).

[7] R. Colbeck and R. Renner, Nat. Phys. **8**, 450 (2012).

[8] M. Giustina, A. Mech, S. Ramelow, B. Wittmann, J. Kofler, J. Beyer, A. Lita, B. Calkins, T. Gerrits, S. W. Nam, R. Ursin, and A. Zeilinger, Nature (London) **497**, 227 (2013).

[9] B. G. Christensen, K. T. McCusker, J. B. Altepeter, B. Calkins, T. Gerrits, A. E. Lita, A. Miller, L. K. Shalm, Y. Zhang, S. W. Nam, N. Brunner, C. C. W. Lim, N. Gisin, and P. G. Kwiat, Phys. Rev. Lett. **111**, 130406 (2013).

[10] M. Giustina, M. A. M. Versteegh, S. Wengerowsky, J. Handsteiner, A. Hochrainer, K. Phelan, F. Steinlechner, J. Kofler, J.-Å. Larsson, C. Abellán, W. Amaya, V. Pruneri, M. W. Mitchell, J. Beyer, T. Gerrits, A. E. Lita, L. K. Shalm, S. W. Nam, T. Scheidl, R. Ursin, B. Wittmann, and A. Zeilinger, Phys. Rev. Lett. **115**, 250401 (2015).

[11] L. K. Shalm, E. Meyer-Scott, B. G. Christensen, P. Bierhorst, M. A. Wayne, M. J. Stevens, T. Gerrits, S. Glancy, D. R. Hamel, M. S. Allman, K. J. Coakley, S. D. Dyer, C. Hodge, A. E. Lita, V. B. Verma, C. Lambrocco, E. Tortorici, A. L. Migdall, Y. Zhang, D. R. Kumor, W. H. Farr, F. Marsili, M. D. Shaw, J. A. Stern, C. Abellan, W. Amaya, V. Pruneri, T. Jennewein, M. W. Mitchell, P. G. Kwiat, J. C. Bienfang, R. P. Mirin, E. Knill, and S. W. Nam, Phys. Rev. Lett. **115**, 250402 (2015).

[12] J. F. Clauser, M. A. Horne, A. Shimony, and R. A. Holt, Phys. Rev. Lett. **23**, 880 (1969).

[13] Y. Liu, X. Yuan, M.-H. Li, W. Zhang, Q. Zhao, J. Zhong, Y. Cao, Y.-H. Li, L.-K. Chen, H. Li, T. Peng, Y.-A. Chen, C.-Z. Peng, S.-C. Shi, Z. Wang, L. You, X. Ma, J. Fan, Q. Zhang, and J.-W. Pan, Phys. Rev. Lett. **120**, 010503 (2018).

[14] L. Shen, J. Lee, L. P. Thinh, J.-D. Bancal, A. Cerè, A. Lamas-Linares, A. Lita, T. Gerrits, S. W. Nam, V. Scarani, and C. Kurtsiefer, Phys. Rev. Lett. **121**, 150402 (2018).

[15] V. Caprara Vivoli, P. Sekatski, J.-D. Bancal, C. C. W. Lim, B. G. Christensen, A. Martin, R. T. Thew, H. Zbinden,

N. Gisin, and N. Sangouard, Phys. Rev. A **91**, 012107 (2015).
[16] M. Takeoka, R.-B. Jin, and M. Sasaki, New J. Phys. **17**, 043030 (2015).
[17] K. P. Seshadreesan, M. Takeoka, and M. Sasaki, Phys. Rev. A **93**, 042328 (2016).
[18] B. Cirelson, Lett. Math. Phys. **4**, 93 (1980).
[19] P. H. Eberhard, Phys. Rev. A **47**, R747 (1993).
[20] R.-B. Jin, R. Shimizu, K. Wakui, M. Fujiwara, T. Yamashita, S. Miki, H. Terai, Z. Wang, and M. Sasaki, Opt. Exp. **22**, 11498 (2014).
[21] S. Miki, M. Yabuno, T. Yamashita, and H. Terai, Opt. Exp. **25**, 6796 (2017).
[22] D. Klyshko, Sov. J. Quantum Electron. **10**, 1112 (1980).